Surface Potential Switching by Metal Ion Complexation/Decomplexation Using Bipyridinethiolate Monolayers on Gold

Tohru Nakamura,*[,†,‡] Emiko Koyama,[§,‡] Yukihiro Shimoi,[†,‡] Shuji Abe,[†,‡] Takao Ishida,[†,‡] Kiyomi Tsukagoshi,[†,¶] Wataru Mizutani,[†,‡] Hideo Tokuhisa,[§,‡] Masatoshi Kanesato,[§,‡] Ikuyo Nakai,[#] Hiroshi Kondoh,[#] and Toshiaki Ohta[#]

Nanotechnology Research Institute (NRI), National Institute of Advanced Industrial Science and Technology (AIST), 1-1-1 Higashi, Tsukuba, Ibaraki 305-8565, Japan, Nanoarchitectonics Research Center (NARC), National Institute of Advanced Industrial Science and Technology (AIST), 1-1-1 Higashi, Tsukuba, Ibaraki 305-8562, Japan, Synthetic Nano-Function Materials Project (SYNAF), National Institute of Advanced Industrial Science and Technology (AIST), 1-1-1 Umezono, Tsukuba, Ibaraki 305-8568, Japan, Japan Science and Technology Corporation (JST), Honcho 4-1-8, Kawaguchi, Saitama 332-0012, Japan, and Department of Chemistry, The University of Tokyo, Hongo, Tokyo 113-0033, Japan

Received: November 24, 2005; In Final Form: February 24, 2006

Surface potential switching on gold(111) surfaces is induced by complexation/decomplexation reactions of a bipyridine (BP) derivative and palladium(II) chloride, as observed by Kelvin probe force microscopy (KFM). On the basis of the theoretical predictions, a 4-(5-phenylethynyl-2,2′-bipyridine-5′-yl-ethynyl)benzenethiol (PhBP) derivative was synthesized and used as an active monolayer to catch transition metal ions. By using the microcontact printing (CP) technique, micron-size patterned PhBP monolayers, which act as effective hosts to coordinate palladium(II) chloride, were prepared on gold(111) surfaces. The KFM signal decreases by complexation of the Pd(II) chloride in PhBP monolayers and is recovered by removal of Pd ions using an ethylenediamine solution, as confirmed by X-ray photoelectron spectroscopy. This process is reversible, indicating that the surface potential switching is realized by complexation/decomplexation of Pd(II). A CP PhBP monolayer, when it detects the target palladium ion, shows sensitivity for the picomolar level detection judged from surface potential changes in KFM measurements. The dipole moment estimated by the surface potentials is much smaller than the calculated value, indicating that mechanisms for the reduction of the surface dipole moment exist in real monolayers prepared by the CP method.

Introduction

Complexation/decomplexation of ions on solid surfaces is crucial to the clarification of host/guest chemistry and its physics at interfaces as well as the technological applications, considering their relation to the construction of sensitive, selective, and cost-effective chemical sensors and memories.

Along these lines, functionalized self-assembled monolayers (SAMs) have extensively been studied in many fields because of their ease of preparation and the variations of head and anchoring groups to control their properties.[1] SAMs using protonatable/deprotonatable molecules have been investigated thoroughly as pH-sensing systems.[2] Adsorbates with selective ligands immobilized on gold were used for the detection of metal ions such as copper,[3] cadmium,[4] mercury,[5] and the other transition metal ions.[4,6] Alkali ion (e.g., Na^+, K^+) detection was also investigated using the SAMs consisting of crown ether derivatives.[7] Inclusion of molecules such as ferrocene, azo, quinine, and phenylalanine derivatives was applied by using cyclodextrin SAMs to detect these guest molecules.[8] It is possible to fabricate the inverse sensing SAMs, which means that SAMs formed by guest molecules in the sense of host/guest chemistry and the target guests are host molecules such as cyclodextrin and crown ether analogues.[9] Still another approach is to sense the sizes of guest complexes by the control of defects or templates in host SAMs—like a SAM sieve.[10] Steric hindrance using a dendrimer was also studied to change the permeability of the ferric complex.[11] In connection with switching performance, SAMs of pyridylazothiol were used for the chelation and release of zinc porphyrin molecules in a toluene solution by using evanescent-field light.[12]

Ion channel sensors (ICSs) using organic SAMs have been under development for the past two decades,[13] which receive considerable attention due to the industrial and medical applications for the sensing system as well as the fundamental research to clarify the reaction mechanism on the surfaces. ICSs detect a change of electrochemical current of redoxactive marker ions coexisting in the sensing system based on host−guest chemistry of specific SAMs on the electrodes. The interaction between host SAMs and guest ions or organic molecules affects the access of redoxacitive marker ions to change the current depending on the concentration of guests.

Sensors having a transistor structure have been widely researched since 1970.[14] A metal oxide semiconductor field effect transistor (MOS-FET) was used to detect hydrogen gas using Pd thin layers as a gate channel.[15] Ion-sensitive field effect transistors (ISFETs) have been amply studied using cast films or membranes on gate to change the potential, which leads to

* To whom correspondence should be addressed. Tel. and fax: +81-29-861-4669; e-mail: tohru.nakamura@aist.go.jp.
† NRI, AIST.
§ NARC, AIST.
‡ SYNAF, AIST.
¶ JST.
# Department of Chemistry, The University of Tokyo.

10.1021/jp056821d CCC: $33.50
Published on Web 04/15/2006

the current change between source and drain.[16] A different type of sensor, the so-called molecular controlled semiconductor resistor (MOCSER), was developed to detect NO gas using hinged iron−chlorophyll derivative monolayers on GaAs.[17]

The guests on these SAMs can be detected primarily by electrochemical techniques (cyclic voltammetry, impedance spectroscopy) as well as wettability measurements (contact angle measurements), mass detection (quartz crystal microbalance (QCM), surface acoustic wave devices (SAWs), secondary ion mass spectroscopy (SIMS)), spectroscopic measurements (IR, UV, fluorescence, ellipsometry, SPR, XPS, AES, and XAFS), and scanning probe microscopy. The combined results of these techniques allow us to understand well the species at the interface and the sensing mechanism of SAMs.

The Kelvin probe technique is a classical method using a Kelvin capacitor to evaluate surface states, especially the difference of the work function or surface potential between two kinds of conductive millimeter- to centimeter-scaled surfaces. By using this method, it was found that the surface potential varied linearly with increasing chain length in alkanethiolate SAMs on gold.[18] Furthermore, a sensing behavior for trialkylamine gas was investigated using porphyrin derivative SAMs and sapphyrin LB films.[19] In comparison, Kelvin probe force microscopy (KFM), one of the SPM techniques, is an advanced method to map surface potentials and dipoles in micro- and nanometer areas. It was also found that KFM signals are associated with the magnitude of a 2-D dipole consisting of the SAMs.[20] KFM measurements enable us to clarify a surface dipole for SAMs on metal. They also estimate work function changes when compared with a control of surfaces in small areas. The control of the 2-D dipole is particularly important to determine the growth process, quality, stability, and properties of SAMs.[21] By KFM techniques, dipole switching of domains consisting of a thin film of ferroelectric copolymers was performed applying a high electric field between a gold-coated cantilever and a conductive substrate.[22] Monolayers prepared from organic silane derivatives on silicon wafers have been studied by KFM.[23] Recently, memory phenomena using surface potential in a microscale region were observed by the oxidation/reduction reactions of aminophenylsilane SAMs on silicon wafers using a KFM cantilever.[24] Despite the high potential and applicability probed by these KFM studies, a complexation/decomplexation of metal ions has not hitherto been reported on solid surfaces by KFM. We report here the switching behavior of phenylethynylbipyridine derivative SAMs as a function of surface potential employing a palladium complex as a guest molecule by Kelvin probe force microscopy. Theoretical predictions for this PhBP system and the photoemission spectroscopies such as XPS and NEXAFS are helpful to understand KFM results on the PhBP-monolayer system. The combined results are meaningful to comprehend the mechanism of surface potential and surface dipole switching by complexation/decomplexation of the metal ion at the interface.

Experimental Procedures

General. Single-crystal Au(111) surfaces with a diameter of 1 cm and a thickness of 1 mm were used and recycled for XPS, NEXAFS, and KFM measurements. The Au(111) surfaces were washed step by step with Piranha, MilliQ water, sodium hydroxide solution, MilliQ water, hydradine monohydrate, fresh MilliQ water twice, distilled ethanol, and distilled tetrahydrofuran and stored in distilled ethanol. The washed surfaces were hydrogen-flamed before usage. PhBP analogues were synthesized and purified using gel permeation chromatography and/or recrystallization. The obtained compounds were identified by ^{1}H NMR and IR. ^{1}H NMR spectra were recorded on a Bruker AF-500 spectrometer using tetramethylsilane (TMS) as an internal standard in chloroform-*d* ($CDCl_3$). IR spectra were obtained with a JASCO FT/IR 420. The elastomeric stamps for microcontact printing were prepared by pouring a mixture of poly(dimethylsiloxane) (PDMS) and its curing agent onto a master silicon wafer with the negative of the desired surface, subsequently by heating at 60 °C for ca. 12 h. The obtained stamps were rinsed several times with ethanol and dioxane. Benzenethiol derivatives were provided by the deprotection of corresponding thioacetate derivatives in dioxane (2.8 mM) using 1.1 equiv of pyrrolidine in ethanol (4.2 mM) at room temperature. A drop of the freshly prepared solution containing thiol was immediately placed on top of the rinsed stamp, with enough liquid covering the surface for about 20 s. Residual solution on top of the PDMS stamp was blown off using a N_2 jet. In the case of KFM measurements, the monolayer transfer of PhBP was realized by microcontact printing using the stamp with micron-size convex−concave patterns on single-crystal gold(111) surfaces placed on a hot plate at ca. 50 °C for 30 min. Afterward, the substrates were rinsed with tetrahydrofuran (THF) to remove physisorbed species. In the case of photoemission spectroscopy such as X-ray photoelectron spectroscopy (XPS) and near-edge X-ray absorption fine structure (NEXAFS), flat PDMS stamps with no micropatterns were used to compare the adsorption states and the coverage with a control. The complexation was performed by the immersion of contact-printed surfaces in a methylene chloride solution of bis(acetonitrile)dichloropalladium(II) ($PdCl_2AN_2$) or a water/methanol/THF (1:1:1) solution of copper(II), nickel(II), iron(II), or iron(III) chloride for a few seconds. Freshly prepared ethylenediamine (EDA) in methylene chloride solution (concentration 5−10 mM) was used to remove the complex in the monolayers. The obtained surfaces were subsequently rinsed by THF and dried by a nitrogen jet.

4-(5-Phenylethynyl-2,2′-bipyridinyl-5′-yl-ethynyl)benzenethioacetate. This compound was synthesized in dry THF by the Sonogashira reaction of the corresponding 5-phenylethynyl-5′-ethynyl-2,2′-bipyridine with 4-iodobenzenethioacetate in the presence of triethylamine: pale yellow solid, ^{1}H NMR ($CDCl_3$): $\delta = 2.45$ (s, 3H, $CH_3C(O)S$-), 7.38−7.39 (m, $3H_{arom}$), 7.44 (d, $J = 8.4$ Hz, $2H_{arom}$), 7.57−7.59 (m, $2H_{arom}$), 7.60 (d, $J = 8.4$ Hz, $2H_{arom}$), 7.95 (dd, $J_1 = 8.3$ Hz, $J_2 = 2.0$ Hz, $2H_{arom}$), 8.45 (dd, $J_1 = 8.3$ Hz, $J_2 = 2.0$ Hz, $2H_{arom}$), 8.82 (brs, $2H_{arom}$). IR (KBr): $\nu = 2216, 1709, 1582, 1528, 1489, 1461, 1364, 1351, 1129$ cm^{-1}

Theoretical Calculations. Density functional theory calculations were carried out using the B3LYP hybrid functional.[25] The effective core potential LanL2DZ was applied to a Pd atom,[26] and a 6-31G(d) basis set was used for other atoms. Structures were fully optimized in vacuo. Charge distribution was analyzed by the natural population analysis.[27] All the calculations were performed using Gaussian 03, Revision B.04.[28]

Surface Analyses. Kelvin probe force microscopic (KFM) measurements were performed to research the surface potentials of PhBP analogues on gold using a SPA300HV (Seiko Instruments Incorporation (SII)) instrument under nitrogen. The distances and heights in the images were calibrated using a 1 μm period calibration grid. Commercially available Rh-coated cantilevers with a spring constant of 2.6 N/m and a resonance frequency in the range of 20−23 kHz were used for the KFM observations. The *Q* factor of the cantilever was approximately 150. The scan rates were around 0.3 Hz in a 30 μm square

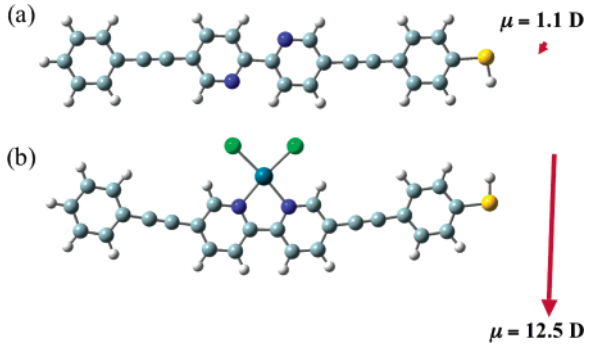

Figure 1. Optimized structures of the PhBP derivatives. (a) PhBP thiol and (b) its complex with $PdCl_2$. Red arrows indicate electric dipole moments.

region. XPS spectra were taken to study the chemical species on gold. The spectra were recorded to check the reproducibility with hemispherical electron analyzers of the theta probe XPS (Thermo VG Scientific) using Al Kα radiation or of Gamma-data-Scienta (SES-2002) on the soft-X-ray beam line 7A at the Photon Factory (Tsukuba) under high vacuum conditions, which covers the photon-energy range of 100−1000 eV. All XPS data were collected at the normal emission angle. All binding energies were calibrated using the Au $4f_{7/2}$ peak (84.0 eV). The NEXAFS experiments were carried out to study the orientation of molecules on gold at the soft X-ray beam line 7A of the Photon Factory in the Institute of Materials Structure Science, High-Energy Accelerator Research Organization (KEK-PF). Nitrogen K-edge NEXAFS spectra were obtained by the partial electron yield method using a microchannel plate (MCP) with a retarding voltage of 300 V in an ultrahigh vacuum chamber. The photon polarization dependence of the NEXAFS spectra was studied using three different photon incident angles of 90° (normal incidence), 55° (magic angle), and 15° (grazing incidence) with respect to the surface.

Results

Theoretical Analyses. To construct molecular switching or sensing systems using bipyridine (BP), the complexation of the BP molecules with metal ions was analyzed by the density functional theory calculations. We selected palladium(II) chloride as a guest, as it forms one of the most stable bondings with BP. The 4-(5-phenylethynyl-2,2′-bipyridine-5′-yl-ethynyl)-benzenethiol (PhBP) molecule was chosen as a host, considering the adsorption and orientation on the Au(111) surface. The optimized structures in Figure 1 show that a stable complex of PhBP is formed with a square-planar configuration of Pd. The complexation changes the conformation of the bipyridine moiety from a trans to cis form and gives rise to a slight bending of the PhBP molecule. This complexation is accompanied by a drastic change of a static electric dipole moment, enhancing its magnitude from 1.1 to 12.5 D. The dipole of the complex is directed almost perpendicular to the molecular long axis as shown in Figure 1. According to the natural population analysis, the electronic charges on Pd and Cl atom are +0.70 and −0.52, respectively, while the BP molecule is charged totally as +0.34. These charge distributions lead to a remarkable change of the dipole moment in the molecule. These findings imply that the complexation as shown in Figure 1 has the possibility of changing the 2-D dipole and the surface potential of metals covered by the BP molecules remarkably if the molecules are appropriately oriented on the surface.

The core levels of nitrogen in PhBP were next estimated in connection with XPS spectroscopy. Our preliminary results of

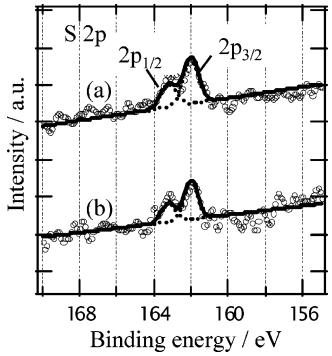

Figure 2. S 2p photoelectron spectra from PhBP monolayers. (a) As prepared and (b) after recycling of PhBP monolayers.

SCHEME 1: Deprotection Reaction of 4-(5-Phenylethynyl-2,2′-bipyridinyl-5′-yl-ethynyl)-benzenethioacetate with Pyrrolidine

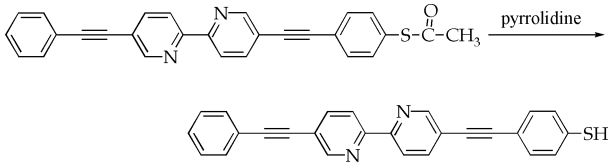

the calculation indicate the shift of the XPS signal toward a higher binding energy after the complexation. This is consistent with the XPS measurements that follow.

XPS Measurements. XPS spectra were studied to confirm the complexation/decomplexation of palladium chloride on the surface. Before the usage for microcontact printing (CP) to transfer the monolayers, the acetyl group for the protection of the PhBP molecule is deprotected by pyrrolidine to provide PhBP thiol in the solutions, as shown in Scheme 1.[29]

Figure 2a shows S 2p photoelectron spectra from a PhBP thin film prepared on gold(111) by a CP stamp. The S $2p_{3/2}$ peak is evident at 162 eV. The S 2p signals remain unchanged as shown in Figure 2b after the complexation/decomplexation described next.

Figure 3 shows core level photoelectron spectra for the other elements; N 1s, Pd 3d, and Cl 2p. The spectra from PhBP monolayers as prepared by CP are shown in Figure 3a,d,g, where the N 1s peak for bare nitrogen of the BP moiety is located at 398.3 eV and no Pd and Cl peaks are observed. A small shoulder in the N 1s spectrum (Figure 3a) is seen at higher binding energy (ca. 400 eV), which is probably caused by contamination or a coordination species of BP onto the gold surface. Drastic changes are observed after immersing in a bis(acetonitrile)-dichloropalladium (II) ($PdCl_2AN_2$) methylene chloride solution and rinsing. In the N 1s spectrum, a distinct peak is observed at a higher binding energy, concomitant with the signal of free PhBP (Figure 3b). Next, Pd $3d_{3/2}$ and $3d_{5/2}$ are seen at ca. 343.5 and 338.2 eV (Figure 3e), and Cl $2p_{3/2}$ is seen at around 197.8 eV (Figure 3h).

The next step is a removal of palladium chloride coordinated in PhBP monolayers by using amine derivatives. We found that ethylenediamine (EDA) is an effective removal reagent of the palladium ion. After the immersion of PhBP−$PdCl_2$ complex monolayers (Figure 3b,e,h) in the EDA solution, all the spectra return to the initial stage (Figure 3c,f,i). During this procedure, the S 2p signals remain unchanged (Figure 3b). Figure 4 summarizes the complexation/decomplexation phenomena of the Pd complex in PhBP monolayers, where the reversible XPS intensity changes are observed for N 1s, Pd 3d, and Cl 2p spectra by Pd(II)-complexation/decomplexation.

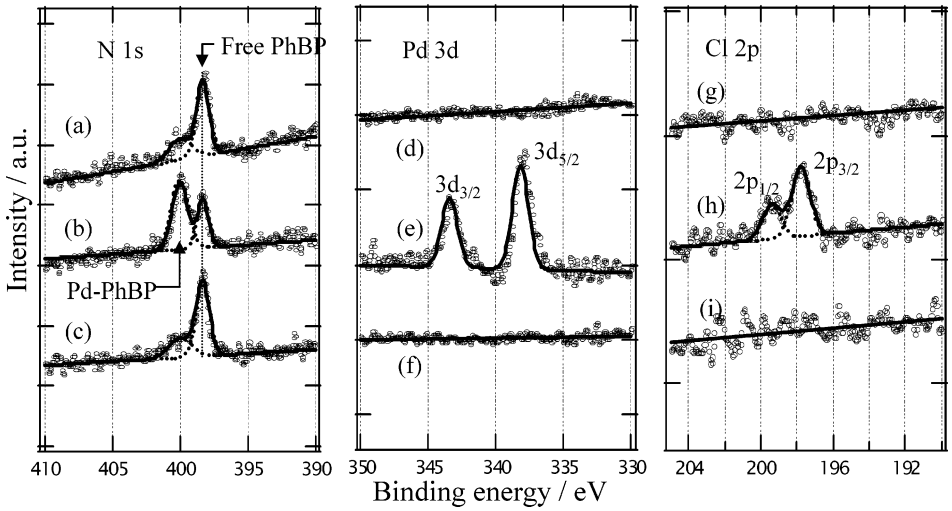

Figure 3. Core level XPS N 1s, Pd 3d, and Cl 2p spectra for PhBP monolayers. (a) N 1s as prepared, (b) N 1s after the interaction with Pd complex, (c) N 1s after the reaction with EDA, (d) Pd 3d as prepared, (e) Pd 3d after the interaction with Pd complex, (f) Pd 3d after the reaction with EDA, (g) Cl 2p as prepared, (h) Cl 2p after the interaction with Pd complex, and (i) Cl 2p after the reaction with EDA.

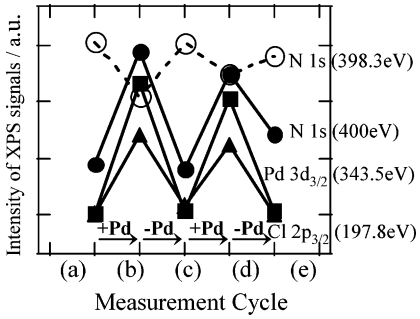

Figure 4. Core level XPS intensity changes for each element. Open circles: N 1s at 398.3 eV (free PhBP); filled circles: N 1s at 400 eV (PhBP−Pd complex), filled squares: Pd $3d_{3/2}$ at 343.5 eV; filled triangles: Cl $2p_{3/2}$ at 197.8 eV.

NEXAFS Measurements. With the aim of understanding a surface dipole, we performed near-edge X-ray absorption fine structure (NEXAFS) analysis that is a powerful method to determine the orientation and average tilt angle of organic monolayers on metal surfaces from a single sample.

N K-edge NEXAFS spectra were investigated to focus on the bipyridine moiety in the PhBP monolayers. Figure 5a shows N K-edge NEXAFS spectra from PhBP monolayers prepared by CP. Two prominent peaks observed around 398 and 407 eV are attributed to the excitations from N 1s to a π^{*1} and a σ^*(C−N) state, respectively.[30] The spectrum shows a weak and broad signal at around 415−420 eV, which is associated with an excitation to a higher lying σ^* orbital.[31]

It is found that pyridine rings adopt a relatively upright configuration judged from the π^{*1} peak at 397.7 eV. The average tilt angle of the pyridine ring before the Pd complexation is quantitatively estimated from polarization dependence of the π^{*1} peak intensity. The peak intensity was obtained by curve-fitting analyses with Gauss functions in addition to a step function, which represents the transition to the continuum states. Polarization dependence for a transition moment with a tilt angle of α is expressed as

$$I \propto \frac{1}{3}P\left[1 + \frac{1}{2}(3\cos^2\beta - 1)(3\cos^2\alpha - 1)\right] + \frac{1}{2}(1 - P)\sin^2\alpha,$$

where β is the polarization angle between the electric vector and the surface normal and P is the polarization factor, 0.94 for the present case.[32] Since the electric vector of the X-ray is

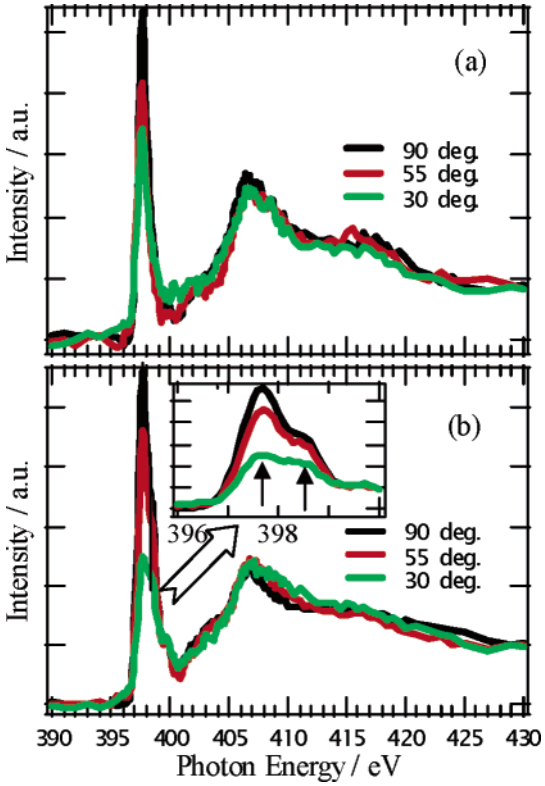

Figure 5. N−K NEXAFS spectra from PhBP monolayers. Three different photon incident angles with respect to the surface are used; 90° (black line), 55° (red line), 15° (green line). (a) As prepared and (b) after the complexation of $PdCl_2$. Inset in panel b: spectra in the range of 396−400 eV in an enlarged scale.

parallel to the plane formed by surface normal and the path of the incident X-ray beam, β is consequently equal to the X-ray incident angle from the surface parallel in Figure 5. From the tilt angle α of transition moment obtained by the ratio of the peak intensities I at three incident angles β (Figure 5a), the tilt angle φ of the pyridine ring was estimated to be 25 ± 5° from surface normal as shown in Figure 10. A remarkable change of the pyridine orientation is observed in the π^* excitation at 397.7 eV as shown in Figure 5b after the palladium complex formation. The signal at 397.7 eV is divided into two components at 397.6 and 398.5 eV (Figure 5b, inset). The tilt angles φ of pyridine rings observed at 397.6 and 398.5 eV after the

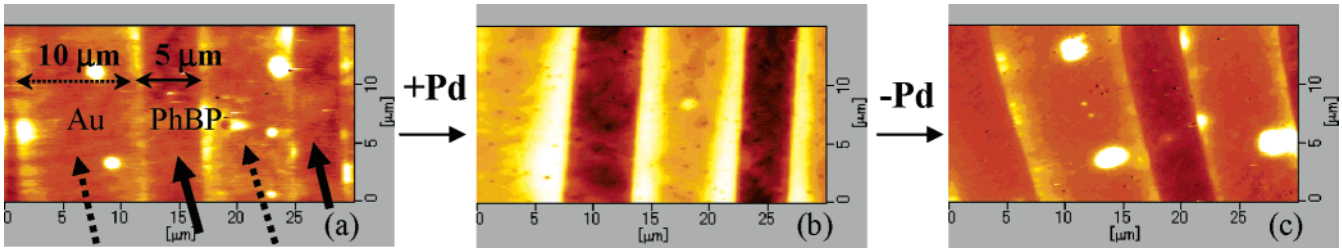

Figure 6. KFM images for the microcontact printing patterns (5/10 μm) consisting of PhBP monolayers. (a) CP patterns as prepared. PhBP molecules chemisorb on the lines with 5 μm width (solid arrows), while the lines with a 10 μm width are bare gold surfaces (dashed arrows). (b) After the immersion in $PdCl_2AN_2$ solution (concentration: 3 mM) and rinsing. (c) After washing with EDA.

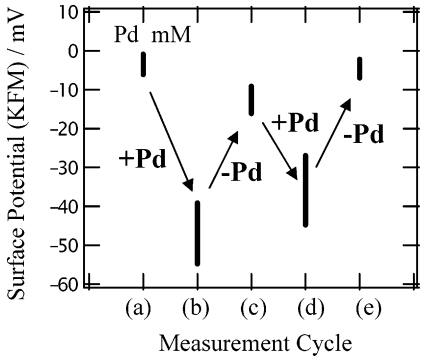

Figure 7. Switching process of CP PhBP monolayers observed by KFM. (a) As prepared and (b) after coordinating with $PdCl_2$ (concentration: 3 mM) and rinsing. (c) After washing with EDA. (d) After coordinating again with $PdCl_2$ (concentration: 3 mM) and rinsing. (e) After washing again with EDA.

complexation are estimated to be 16 ± 5 and 29 ± 5° from surface normal, respectively, by using each polarization dependence of the peak intensities.

KFM Measurements. To detect surface potential and dipole changes of PhBP monolayers prepared by CP, we next performed KFM measurements.

Figure 6 shows the result of surface potential switching for microcontact-printed PhBP monolayers measured by KFM. The areas indicated by solid arrows correspond to PhBP monolayers patterned by CP (a 5 μm convex part of stamp, Figure 6a) and those indicated by dashed arrows, bare gold surfaces (a 10 μm concave part of stamp, Figure 6a). The formation of BP thiolate monolayers and BP-chelating Pd complexes was confirmed by XPS measurements for the samples of KFM, which are in good agreement with the XPS results mentioned in the XPS section. PhBP monolayers show a surface potential of −1 to −6 mV against bare gold as shown in Figure 6a before complexation of Pd(II). After the complexation of Pd(II) using the solution of 3 mM $PdCl_2$, KFM exhibits a drastic reduction of the surface potentials to ca. −50 mV (Figure 6b). The changes of surface potential in KFM measurements sometimes showed sample dependence (e.g., a CP−PhBP monolayer exhibited a surface potential change more than −100 mV, while the other monolayer exhibited a potential change around −20 mV after the interaction of Pd(II)).

Next, the chelated Pd(II) is removed from these BP monolayers' patterns by using EDA. The reduction of surface potential is recovered by EDA, as shown in Figure 6c. The potential of PhBP monolayer pattern can be switched in the KFM measurements. Figure 7 summarizes the switching process of PhBP monolayers as a function of surface potentials at mmol levels of concentration of the Pd complex.

The nanometer level thickness of the organic monolayers can extend the detection limit to a lower concentration due to the direct transport of surface change to the interface. In fact, an efficient KFM change is observed by using CP patterns (Figure 8), in which a diluted Pd solution (μmol/L) is used. Figure 9 also summarizes the switching process of PhBP monolayers as a function of surface potential at the μmol level concentration of Pd. As far as the sensitivity is concerned, we have attained a top record of pM (10^{-12} mol/L, ppt level) detection of the Pd complex in this system. A surface potential decrease of ca. 4 mV was observed after the interaction with 39 pM Pd(II) chloride solution on a CP PhBP monolayer and was recovered by using the EDA solution.

Selectivity of this system was investigated by using different transition metal ions such as copper, iron, and nickel. According to the KFM experiments, Ni(II) and Fe(III) chloride exhibited a significant change of the surface potential, which dropped to ca. −30 and −15 mV, respectively, by using CP−PhBP patterns. In contrast, Cu(II) and Fe(II) showed no significant changes as a preliminary result.

Discussion

Complexation/Decomplexation of PhBP Monolayers Prepared by CP Technique. Theoretical analyses suggest an effective trapping of $PdCl_2$ by PhBP. This is proven by the XPS measurements of 2-D PhBP molecular sheets for each element. The S $2p_{3/2}$ peak at 162 eV in Figure 2 clearly indicates the formation of sulfur−gold covalent bonds on the surface. This means that the PhBP molecule is appropriately fixed on the gold surface. The higher position of N 1s XPS after the interaction of PhBP monolayers with Pd(II) is in good agreement with the XPS peaks of a simple bipyridine−palladium(II) complex.[33] Theoretical analysis on the shift of N 1s XPS is also consistent with this result. The positive charge of the Pd ion adjacent to N of PhBP is considered to be a main reason for the shift of the N 1s peak to a higher binding energy. Next, Pd $3d_{3/2}$ and $3d_{5/2}$ are seen at ca. 343.5 and 338.2 eV (Figure 3e) and Cl $2p_{3/2}$ at around 197.8 eV (Figure 3h). Pd 3d XPS for simple BP−Pd(II) complexes shows the same peak positions.[33] These provide firm evidence of the existence of BP−palladium chloride complexes on the surface. Since the $PdCl_2AN_2$ species spin-coated on the gold surfaces show different peak positions at ca. 342.5 and 347 eV for Pd 3d, obtained results clearly indicate the formation of a molecular thiolate sheet consisting of the PhBP−$PdCl_2$ complex on the surface. CP PhBP monolayers smoothly catch palladium chloride to form the complex of PhBP−$PdCl_2$ on the gold surface, as is consistent with the theoretical prediction.

The contact-printed PhBP monolayers are successfully recyclable for the catch/release of guest complexes by using EDA, which is an effective removal reagent of the palladium ion, as summarized in Figure 4. After the immersion of PhBP−$PdCl_2$ complex monolayers in EDA solution, all the spectra return to the first stage (Figure 3c,f,i). Obtained reset monolayers can be used for the catching of palladium complex again. During this

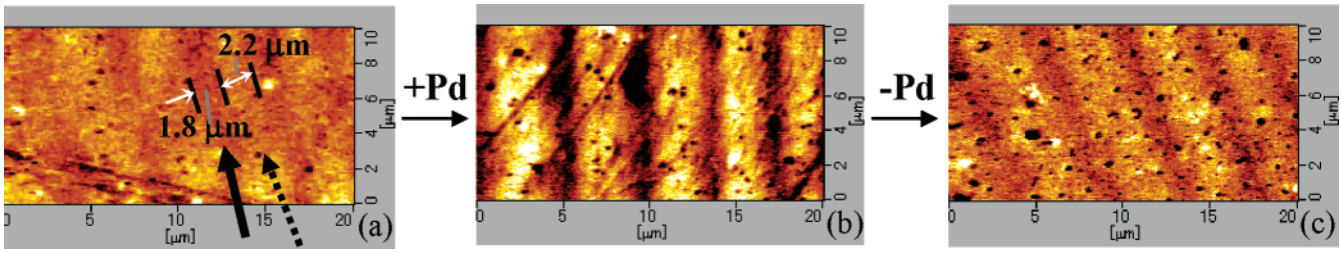

Figure 8. KFM images for the microcontact printing patterns (1.8/2.2 μm) consisting of PhBP monolayers. (a) CP patterns as prepared, PhBP molecules chemisorb on the lines with 1.8 μm width (solid arrow). The lines with 2.2 μm width are bare gold surfaces (dashed arrow). (b) After the immersion in $PdCl_2AN_2$ solution (concentration: 34 μM) and rinsing. (c) After washing with EDA.

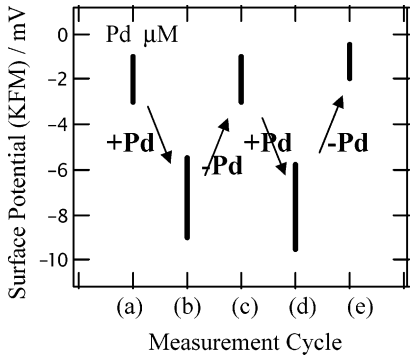

Figure 9. Switching process of CP PhBP monolayers observed by KFM. (a) As prepared and (b) after coordinating with $PdCl_2$ (concentration: 34 μM) and rinsing. (c) After washing with EDA. (d) After coordinating again with $PdCl_2$ (concentration: 34 μM) and rinsing. (e) After washing again with EDA.

procedure, S 2p signals remain unchanged as shown in Figure 2b. These results indicate the possibility of switching and/or recycling the 2-D PhBP molecular system by the complexation/decomplexation of transition metal ions. A proposed process for the complexation/decomplexation in PhBP monolayers is depicted in Figure 10 from the results of XPS measurements.

Molecular Density and Orientation of PhBP Monolayers Prepared by CP Technique. The XPS and NEXAFS measurements revealed that the bipyridine rings in PhBP monolayers prepared by CP adopt an appropriately lower coverage (ca. 74% vs alkanethiolate SAMs), a relatively large tilt angle θ of PhBP molecular long axis (ca 50°), and an upright configuration of bipyridine rings (tilt angle φ around 25°) as mentioned next. A structure model of the PhBP monolayers is schematically illustrated in Figure 10.

The intensity ratio of S 2p and Au 4d peaks of CP PhBP monolayers against the saturated phase of octanethiolate SAMs was estimated by XPS measurements to be 0.46 and 0.62, respectively. From these results, contact-printed PhBP molecules adopt a relatively lower coverage (ca. 74%) when compared with octanethiolate SAMs prepared by the immersion method. This is in moderate to good agreement with a coverage estimated by the edge jump in NEXAFS measurements as compared with a control.

The orientation of PhBP is estimated on Au(111) by NEXAFS measurements. Unfortunately, an average tilt angle θ for the molecular long axis of PhBP cannot be accurately discussed because of mixing the excitations for benzene, pyridine, and an acetylene group in C K-edge NEXAFS spectra. However, it is possible that the tilt angle θ of the PhBP molecule is estimated by the coverage under the assumption that the relation between tilt angle and coverage of alkanethiol is applied for a PhBP molecule. In general, the average tilt angles θ depend on the surface coverage of alkanethiolate on various metal surfaces.[34] The molecular area before the complexation is estimated to be 0.27 nm^2/molecule by the XPS signal ratios described previously so that the average tilt angle θ of PhBP is around 50° from surface normal according to ref 34. The relatively large tilt angle is consistent with the tendency of tilt angles for the benzenethiolate derivatives on gold surfaces.[35] We suppose that the average tilt angle θ is preserved after the complexation as there are no drastic changes of features in N−K NEXAFS spectra over 400 eV (Figure 5b) and C−K NEXAFS spectra (data not shown). Although the average tilt angle of PhBP is estimated to be around 50°, the presence of noncoordinating PhBP after the interaction with palladium chloride as shown in Figure 3b suggests the existence of considerable distribution on PhBP molecular orientation, namely, that molecules do not perfectly arrange with the same conformation and configuration.

Next, the orientation of the BP ring is discussed by N−K NEXAFS. Bipyridine rings adopt a relatively upright configuration 25° from surface normal judged from the signal of excitations from N 1s to π^{*1} in Figure 5. This is probably due to the intermolecular interaction in the real monolayers. Interestingly, the signal at 397.7 eV assigned to the excitations from N 1s to a π^{*1} is divided into two components at 397.6 and 398.5

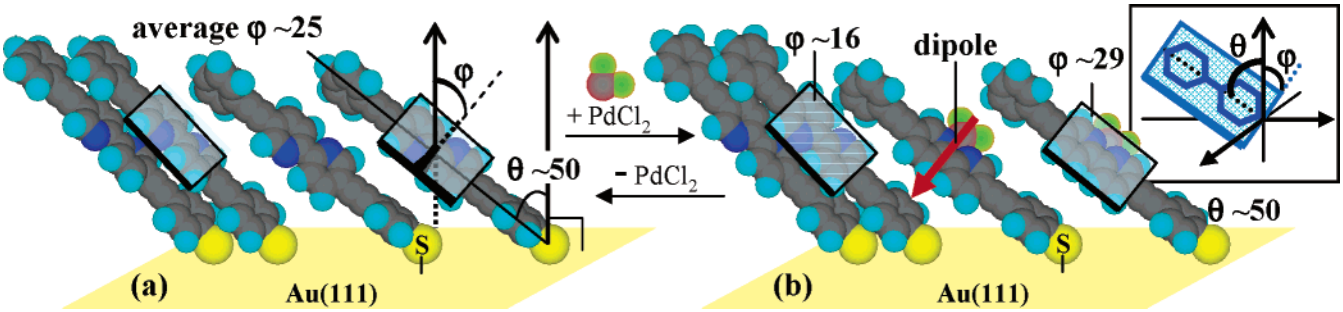

Figure 10. Schematic illustration for adsorption state of CP PhBP molecules in the catch/release reactions on Au(111) surface. Each color corresponds to an element as follows. Black: carbon; sky blue: hydrogen; dark blue: nitrogen; yellow: sulfur; reddish brown: palladium; and light green: chlorine. Red arrow indicates a dipole moment induced in the PhBP−$PdCl_2$ complex. Inset illustrates the orientation of bipyridine ring to understand the tilt angles of θ and φ. The sky blue rectangle indicates the plane of the bipyridine ring.

eV (Figure 5b, inset) after the Pd complexation. The observation of two components for NEXAFS measurements is consistent with those for XPS measurements in which free BP and complex species are observed. We think that the peak at a lower photon energy (397.6 eV) is the signal for the free BP molecule and that the peak at a higher photon energy (398.5 eV) is for the BP−Pd complex when the consistency for XPS results is considered. After the complexation of palladium, the bipyridine rings exhibit a relatively large tilt angle (29°). On the other hand, the remaining free BP rings stand up (tilt angle 16°). These phenomena are presumably due to the stabilization of whole monolayers to relieve repulsive dipole−dipole interactions between Pd−BP molecules, which leads to the increase of occupied areas of Pd−BP molecules and van der Waals interactions.

These results let us consider that the adsorption state of the bipyridine moiety partially contributes to smooth detection of the guest ion and a preservation of the dipole moment of a Pd−PhBP complex in KFM measurements. The information about adsorption states of CP PhBP is useful to consider the results of KFM measurements described next.

Surface Potential and Dipole Changes of PhBP Monolayers. We first discuss the PhBP monolayers from the viewpoint of surface potential. Theoretical analyses indicate the remarkable change of dipole moments after the complexation of the palladium ion with PhBP. In general, a surface potential change ΔV of organic monolayers is directly proportional to molecular dipole changes $\Delta\mu$ directed to surface normal,[20,23] so that it is possible that PhBP molecules exhibit a significant surface potential change.

The enhancement of surface potential change needs the criteria for the orientation and density of PhBP molecules on the surface. In this sense, the PhBP molecule is suited for this purpose because the PhBP molecule as a benzenethiol derivative is expected to adopt the orientation with relatively large tilt angles of the molecular long axis from the surface normal. A large tilt angle of the molecular long axis of PhBP will induce the enhancement of the dipole moment of the PhBP−$PdCl_2$ complex directed to the surface normal. Furthermore, the combination of the relatively large tilt angle of PhBP and the molecular shape having rigid and long phenylacetylene groups will result in keeping enough space for the complexation on the surfaces. Upright configurations of the bipyridine ring are also essential to the introduction of significant dipole changes. No change of surface potential is expected if the BP rings adopt a flat-lying configuration.

The contact-printed PhBP monolayers essentially satisfy the criteria for enhancement of surface potential. This is proven by the KFM and photoemission spectroscopic measurements. The results of XPS indicate that the PhBP monolayers work well to catch/release palladium chloride at the interface. KFM measurements indicate that the surface potential can be switched by complexation/decomplexation of the transition metal ion on the surfaces. We think at present that the decrease of surface potential measured by KFM is correlated with a reduction of work function (i.e., an apparent jump of the Fermi level at the interface or a shift of the vacuum level caused by the complexation on the surface), and they are recovered by the decomplexation.

This is a specific feature of the PhBP monolayers since other surfaces such as bare gold and ultrathin films using other blank systems showed no switching phenomena. Blank tests are of essential importance to clarify the mechanism of KFM phenomena for the PhBP monolayers. Using the same CP technique, KFM measurements were performed for a 4-phenylethynylbiphenylene derivative[36] that has the same molecular dimensions and shape for PhBP and no nitrogen groups. This blank test reproducibly showed no change of the KFM signal before/after immersion in the $PdCl_2AN_2$ solution. Furthermore, no switching phenomenon was observed for the gold surfaces patterned by a CP stamp, which used only organic solvents or only pyrrolidine for the deprotection of the starting PhBP molecule. These results clearly indicate that surface dipole switching discovered in 4-phenylethynylbipyridine monolayers is induced by the complexation/decomplexation of the active center of the bipyridine moiety in PhBP monolayers prepared by the CP technique.

Next to be considered are the actual dipole moments on the surface. While KFM can detect the dipole sheets of SAMs,[20,23] KFM can generally detect the surface potential change or the work function change between different surfaces using the same metal of the KFM cantilever. Again, the surface potential change is theoretically correlated with the dipole moment change of the molecule in monolayers by the following equation: $\Delta V = \Delta\mu/A_{mol}\epsilon_0\epsilon_{mol}$, under the hypothesis that the molecules perfectly align on the surfaces with the same orientation, where $\Delta\mu$ is the change of molecular dipole moment directed normally to the surface, A_{mol} is the area occupied by the unimolecule, and ϵ_0 and ϵ_{mol} are the dielectric constants of free space and organic compounds, respectively. Hence, the obtained results of KFM indicate significant dipole changes and enhanced negative charges of the dipole moment at the top of the PhBP monolayers due to the chloride group by sensing palladium(II) chloride, as deduced from theoretical analyses and XPS measurements. This means that the average dipole moment in PhBP−$PdCl_2$ monolayers directs downward from the top to the vicinity of the gold surface, having a negative value.

The active dipole moment of the contact-printed PhBP monolayers is next estimated from the results of KFM and photoemission measurements. Since the contact printing patterns only consist of bare Au(111) surfaces and PhBP monolayers on Au(111), the surface potential of PhBP monolayers ΔV based on gold is simply expressed by $\mu^1_{PhBP}/A_{PhBP}\epsilon_0\epsilon_{PhBP}$, where μ^1_{PhBP} is the average dipole moment of PhBP molecules directed normally to the surface, A_{PhBP} is the area occupied by the single PhBP molecule, and ϵ_0 and ϵ_{PhBP} are the dielectric constants of free space and PhBP molecules, respectively.[20,23] Therefore, a dipole moment μ_{PhBP} induced in the PhBP molecule after Pd complexation can be estimated by the following equation, considering the orientation of the dipole moment of the PhBP molecules in the monolayers as shown in Figure 10b.[37]

$$\mu_{PhBP} = \Delta V A_{PhBP}\epsilon_0\epsilon_{PhBP}/\sin\theta\cos\varphi$$

where ΔV is the surface potential measured by KFM, and θ and φ are the average tilt angles of the PhBP molecular long axis and bipyridine ring of PhBP from surface normal, respectively. As a result, the induced dipole moment μ_{PhBP} was estimated to be ca. −0.16 D per molecule,[38] whose absolute value is below ca. 1/80 times the value (12.5 D) obtained by calculation.

The following are considered to be reasons for the much smaller dipole induced in real monolayers when compared with calculated value: (1) PhBP−Pd molecules are not perfectly ordered in the real monolayers. PhBP molecules adopt various configurations including a flat-lying configuration with trans-, cis-, or gauche-forms of bipyridine and an upright configuration with a tightly packed arrangement. This means that some of the PhBP molecules can chelate palladium chloride but the others cannot. (2) A steric hindrance of palladium chloride after

the complexation probably inhibits further reaction of PhBP with the ion. These reactivity differences (1) and changes (2) in the real monolayers are suggested in N 1s XPS and N−K NEXAFS measurements. (3) A contamination from air such as water molecules, gas molecules, or volatile organic material cannot be ruled out for the remarkable decrease of the surface dipole density. (4) The repulsive interaction between adjacent dipole moments directing to the same direction leads to a zigzag arrangement of dipoles where dipoles orient in antiparallel or head-to-tail configurations. This canceling of the molecular dipoles in the real film will effectively reduce the surface dipole. (5) A mirror image of the dipole in gold layers against the real molecular dipole on the surface might affect the reduction of the surface dipole. This mechanism is still unclear but is one of the candidates. It is assumed that the combination of these effects (1−5) drastically weakens the total surface dipole consisting of molecules on the surface. To make the dipole moment closer to the theoretical value, we have to develop not only the preparation method for the control of molecular density and orientation but also the equilibrium system of the host/guest at the interface, the adjustment of distance between molecular dipole and surface, and the system to avoid the repulsive interaction between adjacent dipole moments. The control of orientation, arrangement, and reactivity of host molecules by the modification of molecular structures will be crucial to the enhancement for the response of dipole changes when sensing target ions.

The results in the present study imply that further studies are needed to clarify the correlation between surface potential or work function and surface dipole at the vicinity of metal surfaces.

PhBP monolayers prepared by CP showed a sensitivity (pM) and a selectivity for the detection of transition metals although the sample dependence affected the response of the signals. We think that a nanometer level thickness of organic monolayers can extend the detection limit and the speed of response by the direct transport of surface potential change to the interface. The findings on selectivity are intriguing from the viewpoint of sensors, although the scenario of reactions on the surface is still unclear. We suppose that PhBP monolayers possess a potential to distinguish between different transition metal ions due to the different interaction and reactivity of PhBP with each metal ion. The combination of improved sensitivity with specific selectivity using organic monolayers will pave the way for the construction of advanced sensor and chemical memory.

Conclusions

We demonstrate the reversible surface potential changes for bipyridine (BP) derivative monolayers by the catch/release of a target molecule (i.e., palladium(II) complex). XPS and NEXAFS measurements help to illustrate the adsorption states, dipole arrangement, and function of PhBP monolayers on the real surface. Obtained experimental results are essentially compatible with theoretical predictions.

The combined results revealed the mechanism of surface potential switching for contact-printed PhBP monolayers: (1) theoretical analyses indicate that the complexation of PhBP thiol with $PdCl_2$ induces the dipole moment of 12.5 D perpendicular to the molecular axis and predict that the N 1s XPS signal of PhBP shifts at a higher binding energy after the complexation. (2) XPS measurements reveal the Pd complexation/decomplexation of 2-D molecular films consisting of contact-printed PhBP thiolate on Au(111). (3) NEXAFS measurements suggest that the bipyridine moiety in contact-printed PhBP monolayers adopts an upright configuration. (4) It is found by KFM that the dipole arrangement consisting of PhBP thiolate monolayers can be switched by the complexation/decomplexation of transition metal ion on the surfaces; however, the surface dipole changes estimated by KFM surface potential changes are much smaller than the calculated value.

Our demonstration using BP monolayers on the metal surface pointed out aspects such as mechanism, reactivity, arrangement, and orientation of the molecule on the surface to improve the response of organic monolayers toward the construction of advanced devices (e.g., sensor or chemical switching memory combined with microfluidics or the other device structures, which can be recycled and renovated under ambient conditions).

Acknowledgment. This work was supported by the New Energy and Industrial Technology Development Organization (NEDO) under the Nanotechnology Program in Japan. We are deeply grateful for NEDO's support of the Synthetic Nano-Function Materials Project (SYNAF, project leader: Prof. Hiroshi Yokoyama (Ph.D.), Director of Nanotechnology Research Institute (NRI)) in the promotion of this study. A part of this work was conducted at the Nano-Processing Facility of National Institute of Advanced Industrial Science and Technology (AIST-NPF). The present work of NEXAFS has been performed under the approval of the Photon Factory Program Advisory Committee (PF PAC No. 2004G318).

References and Notes

(1) (a) Flink, S.; van Veggel, F. C. J. M.; Reinhoudt, D. N. *Adv. Mater*. **2000**, *12*, 1315. (b) Flink, S.; van Veggel, F. C. J. M.; Reinhoudt, D. N. *Sensor Update* **2001**, *8*, 3.

(2) (a) Hickman, J. J.; Ofer, D.; Laibinis, P. E.; Whitesides, G. M.; Wrighton, M. S. *Science* **1991**, *252*, 688. (b) Cheng, Q.; Brajter-Toth, A. *Anal. Chem*. **1992**, *64*, 1998. (c) Bryant, M. A.; Crooks, R. M. *Langmuir* **1993**, *9*, 385. (d) Zhang, L.; Lu, T.; Gokel, G. W.; Kaifer, A. E. *Langmuir* **1993**, *9*, 786. (e) Takehara, K.; Takemura, H.; Ide, Y. *Electrochim. Acta* **1994**, *39*, 817. (f) Cheng, Q.; Brajter-Toth, A. *Anal. Chem*. **1995**, *67*, 2767. (g) Caldwell, W. R.; Campbell, D. J.; Chen, K.; Herr, B. R.; Mirkin, C. A.; Malik, A.; Durbin, M. K.; Dutta, P.; Huang, K. G. *J. Am. Chem. Soc*. **1995**, *117*, 6071. (h) Cheng, Q.; Brajter-Toth, A. *Anal. Chem*. **1996**, *68*, 4180. (i) Zhao, M.; Tokuhisa, H.; Crooks, R. M. *Angew. Chem., Int. Ed. Engl*. **1997**, *36*, 2596. (j) Casero, E.; Darder, M.; Takada, K.; Abruna, H. D.; Pariente, F.; Lorenzo, E. *Langmuir* **1999**, *15*, 127. (k) Bculen, M. W. J.; van Veggel, F. C. J. M.; Reinhoudt, D. N. *Chem. Commun*. **1999**, 503. (l) Koyama, E.; Ishida, T.; Tokuhisa, H.; Belaissaoui, A.; Nagawa, Y.; Kanesato, M. *Chem. Commun*. **2004**, 1626.

(3) (a) Rubinstein, I.; Steinberg, S.; Tor, Y.; Shanzer, A.; Sagiv, J. *Nature* **1988**, *332*, 426. (b) Steinberg, S.; Rubinstein, I. *Langmuir* **1992**, *8*, 1183.

(4) (a) Steinberg, S.; Tor, Y.; Sabatani, E.; Rubinstein, I. *J. Am. Chem. Soc*. **1991**, *113*, 5176. (b) Turyan, I.; Mandler, D. *Anal. Chem*. **1994**, *66*, 58.

(5) Turyan, I.; Mandler, D. *Nature* **1993**, *362*, 703.

(6) Boiadjiev, V. I.; Brown, G. M.; Pinnaduwage, L. A.; Goretzki, G.; Bonnesen, P. V.; Thundat, T. *Langmuir* **2005**, *21*, 1139.

(7) (a) Moore, A. J.; Goldenberg, L. M.; Bryce, M. R.; Petty, M. C.; Monkman, A. P.; Marenco, C.; Yarwood, J.; Joyce, M. J.; Port, S. N. *Adv. Mater*. **1998**, *10*, 395. (b) Flink, S.; Boukamp, B. A.; van den Berg, A.; van Veggel, F. C. J. M.; Reinhoudt, D. N. *J. Am. Chem. Soc*. **1998**, *120*, 4652. (c) Flink, S.; van Veggel, F. C. J. M.; Reinhoudt, D. N. *J. Phys. Chem. B* **1999**, *103*, 6515. (d) Bandyopadhyay, K.; Liu, H.; Liu, S.-G.; Echegoyen, L. *Chem. Commun*. **2000**, 141. (e) Bandyopadhyay, K.; Shu, L.; Liu, H.; Echegoyen, L. *Langmuir* **2000**, *16*, 2706.

(8) (a) Rojas, M. T.; Königer, R.; Stoddart, J. F.; Kaifer, A. E. *J. Am. Chem. Soc*. **1995**, *117*, 336. (b) Henke, C.; Steinem, C.; Janshoff, A.; Steffan, G.; Luftmann, H.; Sieber, M.; Galla, H.-J. *Anal. Chem*. **1996**, *68*, 3158. (c) He, P.; Ye, J.; Fang, Y.; Suzuki, I.; Osa, T. *Anal. Chim. Acta* **1997**, *337*, 217. (d) Maeda, Y.; Fukuda, T.; Yamamoto, H.; Kitano, H. *Langmuir* **1997**, *13*, 4187. (e) Lee, J.-Y.; Park, S.-M. *J. Phys. Chem. B* **1998**, *102*, 9940. (f) Stine, K. J.; Andrauskas, D. M.; Khan, A. R.; Forgo, P.; D'Souza, V. T. *J. Electroanal. Chem*. **1999**, *465*, 209. (g) Fukuda, T.; Maeda, Y.; Kitano, H. *Langmuir* **1999**, *15*, 1887. (h) Michalke, A.; Janshoff, A.; Steinem, C.; Henke, C.; Sieber, M.; Galla, H.-J. *Anal. Chem*. **1999**, *71*, 2528. (i) Beulen, M. W. J.; Bügler, J.; de Jong, M. R.; Lammerink, B.; Huskens, J.; Schönherr,

H.; Vancso, G. J.; Boukamp, B. A.; Wieder, H.; Offenhäuser, A.; Knoll, W.; van Veggel, F. C. J. M.; Reinhoudt, D. N. *Chem.—Eur. J.* **2000**, *6*, 1176.

(9) (a) Zhang, L.; Godinez, L. A.; Lu, T.; Gokel, G. W.; Kaifer, A. E. *Angew. Chem., Int. Ed. Engl*. **1995**, *34*, 235. (b) Arias, F.; Godínez, L. A.; Wilson, S. R.; Kaifer, A. E.; Echegoyen, L. *J. Am. Chem. Soc*. **1996**, *118*, 6086. (c) Ju, H.; Leech, D. *Langmuir* **1998**, *14*, 300. (d) Sabapathy, R. C.; Bhattacharyya, S.; Cleland, W. E., Jr.; Hussey, C. L. *Langmuir* **1998**, *14*, 3797.

(10) (a) Chailapakul, O.; Crooks, R. M. *Langmuir* **1995**, *11*, 1329. (b) Motesharei, K.; Ghadiri, M. R. *J. Am. Chem. Soc.* **1997**, *119*, 11306. (c) Mirsky, V. M.; Hirsch, T.; Piletsky, S. A.; Wolfbeis, O. S. *Angew. Chem., Int. Ed.* **1999**, *38*, 1108.

(11) Gorman, C. B.; Miller, R. L.; Chen, K.-Y.; Bishop, A. R.; Haasch, R. T.; Nuzzo, R. G. *Langmuir* **1998**, *14*, 3312.

(12) Wang, Z.; Nygrd, A.-M.; Cook, M. J.; Russell, D. A. *Langmuir* **2004**, *20*, 5850.

(13) (a) Umezawa, Y. *Oyo Butsuri (Japanese, Appl. Phys.)* **2000**, *69*, 43. (b) Sugawara, M.; Hirano, A.; Buhlmann, P.; Umezawa, Y. *Bull. Chem. Soc. Jpn*. **2002**, *75*, 187. (c) Umezawa, Y.; Aoki, H. *Anal. Chem*. **2004**, *76*, 320a. (d) Schön, P.; Degefa, T. H.; Asaftei, S.; Meyer, W.; Walder, L. *J. Am. Chem. Soc*. **2005**, *127*, 11486.

(14) Bergveld, P. *IEEE Trans. Biomed. Eng*. **1970**, *17*, 70.

(15) Lundström, I.; Shivaraman, M. S.; Svensson, C.; Lundkuist, L. *Appl. Phys. Lett*. **1975**, *26*, 55.

(16) (a) Matsuo, T.; Wise, K. D. *IEEE Trans. Biomed. Eng*. **1974**, *21*, 485. (b) Moss, S. D.; Janata, J. J.; Johnson, C. C. *Anal. Chem*. **1975**, *47*, 2238. (c) Buck, R. P.; Hackleman, D. E. *Anal. Chem*. **1977**, *49*, 2315.

(17) (a) Wu, D. G.; Cahen, D.; Graf, P.; Naaman, R.; Nitzan, A.; Shvarts, D. *Chem.—Eur. J.* **2001**, *7*, 1743. (b) Ashkenasy, G.; Cahen, D.; Cohen, R.; Shanzer, A.; Vilan, A. *Acc. Chem. Res*. **2002**, *35*, 121.

(18) Evans, S. D.; Ulman, A. *Chem. Phys. Lett.* **1990**, *170*, 462.

(19) D'Amico, A. D.; Natale, C. D.; Paolesse, R.; Mantini, A.; Goletti, C.; Davide, F.; Filosofi, G. *Sens. Actuators, B* **2000**, *70*, 254.

(20) (a) Lue, J.; Delamarche, E.; Eng, L.; Bennewitz, R.; Meyer, E.; Guentherodt, H.-J. *Langmuir* **1999**, *15*, 8184. (b) Lu, J.; Eng, L.; Bennewitz, R.; Meyer, E.; Guntherodt, H.-J.; Delamarche, E.; Scandella, L. *Surf. Interface Anal.* **1999**, *27*, 368.

(21) (a) Kang, J. F.; Ulman, A.; Liao, S.; Jordan, R. *Langmuir* **1999**, *15*, 2095. (b) Liao, S.; Shnidman, Y.; Ulman, A. *J. Am. Chem. Soc.* **2000**, *122*, 3688. (c) Ulman, A. *Acc. Chem. Res*. **2001**, *34*, 855.

(22) Chen, X. Q.; Yamada, H.; Horiuchi, T.; Matsushige, K.; Weiss, P. S. *Mol. Cryst. Liq. Cryst.* **1999**, *A337*, 285.

(23) (a) Saito, N.; Hayashi, K.; Sugimura, H.; Takai, O.; Nakagiri, N. *Chem. Phys. Lett*. **2001**, *349*, 172. (b) Sugimura, H.; Hayashi, K.; Saito, N.; Takai, O.; Nakagiri, N. *J. J. Appl. Phys., Part 2* **2001**, *40* (2B), L174. (c) Sugimura, H.; Hayashi, K.; Saito, N.; Nakagiri, N.; Takai, O. *Appl. Surf. Sci*. **2002**, *188*, 403. (d) Hayashi, K.; Saito, N.; Sugimura, H.; Takai, O.; Nakagiri, N. *Langmuir* **2002**, *18*, 7469. (e) Saito, N.; Hayashi, K.; Sugimura, H.; Takai, O. *J. Mater. Chem*. **2002**, *12*, 2684. (f) Saito, N.; Kadoya, Y.; Hayashi, K.; Sugimura, H.; Takai, O. *J. J. Appl. Phys., Part 1* **2003**, *42* (4B), 2534. (g) Sugimura, H.; Saito, N.; Maeda, N.; Ikeda, I.; Ishida, Y.; Hayashi, K. *Nanotechnology* **2004**, *15*, S69.

(24) Saito, N.; Lee, S.-H.; Ishizaki, T.; Hieda, J.; Sugimura, H.; Takai, O. *J Phys. Chem. B* **2005**, *109*, 11602.

(25) Becke, A. D. *J. Chem. Phys.* **1993**, *98*, 5648.

(26) Hay, P. J.; Wadt, W. R. *J. Chem. Phys.* **1985**, *82*, 299.

(27) (a) Reed, A. E.; Weinhold, F. *J. Chem. Phys.* **1983**, *78*, 4066. (b) Reed, A. E.; Weinstock, R. B.; Weinhold, F. *J. Chem. Phys.* **1985**, *83*, 735. (c) Glendening, E. D.; Reed, A. E.; Carpenter, J. E.; Weinhold, F. *NBO*, Version 3.1.

(28) Frisch, M. J.; Trucks, G. W.; Schlegel, H. B.; Scuseria, G. E.; Robb, M. A.; Cheeseman, J. R.; Montgomery, J. A., Jr.; Vreven, T.; Kudin, K. N.; Burant, J. C.; Millam, J. M.; Iyengar, S. S.; Tomasi, J.; Barone, V.; Mennucci, B.; Cossi, M.; Scalmani, G.; Rega, N.; Petersson, G. A.; Nakatsuji, H.; Hada, M.; Ehara, M.; Toyota, K.; Fukuda, R.; Hasegawa, J.; Ishida, M.; Nakajima, T.; Honda, Y.; Kitao, O.; Nakai, H.; Klene, M.; Li, X.; Knox, J. E.; Hratchian, H. P.; Cross, J. B.; Adamo, C.; Jaramillo, J.; Gomperts, R.; Stratmann, R. E.; Yazyev, O.; Austin, A. J.; Cammi, R.; Pomelli, C.; Ochterski, J. W.; Ayala, P. Y.; Morokuma, K.; Voth, G. A.; Salvador, P.; Dannenberg, J. J.; Zakrzewski, V. G.; Dapprich, S.; Daniels, A. D.; Strain, M. C.; Farkas, O.; Malick, D. K.; Rabuck, A. D.; Raghavachari, K.; Foresman, J. B.; Ortiz, J. V.; Cui, Q.; Baboul, A. G.; Clifford, S.; Cioslowski, J.; Stefanov, B. B.; Liu, G.; Liashenko, A.; Piskorz, P.; Komaromi, I.; Martin, R. L.; Fox, D. J.; Keith, T.; Al-Laham, M. A.; Peng, C. Y.; Nanayakkara, A.; Challacombe, M.; Gill, P. M. W.; Johnson, B.; Chen, W.; Wong, M. W.; Gonzalez, C.; Pople, J. A. Gaussian 03, Revision B.04; Gaussian, Inc.: Pittsburgh, PA, 2003.

(29) The deprotection of PhBP thioacetate was carried out using 1.1 equiv of pyrrolidine in a 1,4-dioxane solution of the BP molecules. The proceeding of the reaction was confirmed in 1,4-dioxane-d_8 by the complete disappearance of the methyl proton signal of the S-protecting acetyl group at ca. 2.4 ppm in the ^{1}H NMR spectra.

(30) (a) Bagus, P. S.; Weiss, K.; Schertel, A.; Wöll, Ch.; Braun, W.; Hellwig, C.; Jung, C. *Chem. Phys. Lett*. **1996**, *248*, 129. (b) Väterlein, P.; Fink, R.; Umbach, E., Wurth, W. *J. Chem. Phys*. **1998**, *108*, 3313.

(31) (a) Horsley J. A.; Stöhr, J.; Hitchcock, A. P.; Newbury, D. C.; Johnson, A. L.; Sette, F. *J. Chem. Phys*. **1985**, *83*, 6099. (b) Bonello, J. M.; Lindsay, R.; Santra, A. K.; Lambert, R. M. *J. Phys. Chem. B* **2002**, *106*, 2672.

(32) Stöhr, J. *NEXAFS Spectroscopy*; Springer: Berlin, 1992.

(33) Hermans, S.; Wenkin, M.; Devillers, M. *J. Mol. Catal., A* **1998**, *136*, 59.

(34) Kondoh, H.; Nambu, A.; Ehara, Y.; Matsui, F.; Yokoyama, T.; Ohta, T. *J. Phys. Chem. B* **2004**, *108*, 12946.

(35) (a) Heister, K.; Rong, H.-T.; Buck, M.; Zharnikov, M.; Grunze, M. *J. Phys. Chem. B* **2001**, *105*, 6888. (b) Whelan, C. M.; Barnes, C. J.; Walker, C. G. H.; Brown, N. M. D. *Surf. Sci.* **1999**, *425*, 195.

(36) 4-(4-Phenylethynyl-biphenyl-4′-yl-ethynyl)benzenethioacetate: this compound was synthesized in dry THF by the Sonogashira reaction of the corresponding 4-phenylethynyl-4′-ethynyl-biphenylene with 4-iodobenzenethioacetate in the presence of triethylamine. Pale yellow solid, ^{1}H NMR ($CDCl_3$): $\delta = 2.44$ (s, 3H, $CH_3C(O)$-), 7.35−7.37 (m, $3H_{arom}$), 7.41 (d, $J = 7.9$ Hz, $2H_{arom}$), 7.55−7.57 (m, $2H_{arom}$), 7.58 (d, $J = 8.0$ Hz, $2H_{arom}$), 7.61−7.62 (br s, $8H_{arom}$). IR (KBr): $\nu = 2216$, 1699, 1498, 1398, 1351, 1126, 1110 cm^{-1}.

(37) The equation refers to the relation between surface potential and molecular dipole moment in refs 20 and 23c,d. The surface-normal component of the dipole moment of PhBP−$PdCl_2$ was deduced considering the tilt angle θ of the PhBP molecular long axis and the tilt angle φ of the bipyridine ring from the surface normal. The tilt angle φ of the bipyridine ring originates from the combination between the rotation of the bipyridine ring around the axis of the acetylene triple bond and the tilt angle θ. Because the dipole moment induced in the PhBP−$PdCl_2$ complex is perpendicular to the molecular long axis, the surface-normal component is increased by sine of the tilt angle θ, and subsequently is decreased by cosine of the ring tilt angle φ.

(38) The following values were used to estimate the dipole moment: ΔV is −50 mV detected by KFM measurements, A_{PhBP} is 0.27 nm^2 estimated by XPS, ϵ_0 is 8.854×10^{-12} C/J m, and φ is 29° from surface normal obtained by NEXAFS under the hypothesis that each dipole adopts the same orientation with a downward direction. Further, 1 D = 3.3×10^{-30} C m, and θ is 50° estimated by the coverage of PhBP in the XPS measurements. ϵ_{PhBP} is 3.0 under the assumption of the general range of dielectric constants for organic compounds.